

Article

Synthesis, Characterization, and Antitumor Mechanism Investigation of Ruthenium(II)/Rhenium(I)-Daminozide Conjugates

Pei-Xin Yang ^{1,†}, Kai Xie ^{1,†}, Mei-Ru Chen ¹, Zheng Zhang ¹, Bo Huang ^{2,*}, Rong-Tao Li ¹ and Rui-Rong Ye ^{1,*} 

¹ Faculty of Life Science and Technology, Kunming University of Science and Technology, Kunming 650500, China

² Faculty of Chemistry and Chemical Engineering, Yunnan Normal University, Kunming 650500, China

* Correspondence: huangbo15@foxmail.com (B.H.); yerr@mail2.sysu.edu.cn (R.-R.Y.)

† These authors contributed equally to this work.

Abstract: Daminozide, a plant growth regulator, is an effective inhibitor of the Jumonji domain-containing protein (JMJD) histone demethylase. Herein, four ruthenium(II)/rhenium(I)-daminozide conjugates, with molecular formulas [Ru(N-N)₂bpy(4-CH₂OH-4'-CH₂O-daminozide)](PF₆)₂ (**Ru-1/Ru-2**) (N-N = 1,10-phenanthroline (phen, in **Ru-1**) and 4,7-diphenyl-1,10-phenanthroline (DIP, in **Ru-2**)) and Re(N-N)(CO)₃(PyCH₂O-daminozide) (**Re-1/Re-2**) (Py = pyridine, N-N = phen (in **Re-1**) and DIP (in **Re-2**)), were synthesized and characterized. Among these complexes, **Ru-2** and **Re-2** exhibited higher cytotoxicity against tumor cells than cisplatin. Upregulation of H3K9Me3 expression level was found in human cervical cancer cells (HeLa) treated with **Ru-2** and **Re-2**, indicating that these two complexes can inhibit the activity of JMJD histone demethylase. Further investigation revealed that **Re-2** can selectively accumulate in the mitochondria of HeLa cells. Both **Ru-2** and **Re-2** can cause mitochondrial damage, induce apoptosis, and inhibit cell migration and colony formation of HeLa cells. Overall, these complexes exhibit multiple anticancer functions, including inhibiting JMJD, inducing apoptosis, and inhibiting cell invasion, making them promising candidates for anticancer drugs.



Citation: Yang, P.-X.; Xie, K.; Chen, M.-R.; Zhang, Z.; Huang, B.; Li, R.-T.; Ye, R.-R. Synthesis, Characterization, and Antitumor Mechanism

Investigation of Ruthenium(II)/Rhenium(I)-Daminozide Conjugates. *Inorganics* **2023**, *11*, 142. <https://doi.org/10.3390/inorganics11040142>

Academic Editors: Wanhe Wang, Duncan Chung-Hang Leung, Jing Wang and Guochen Bao

Received: 10 March 2023

Revised: 20 March 2023

Accepted: 24 March 2023

Published: 26 March 2023



Copyright: © 2023 by the authors. Licensee MDPI, Basel, Switzerland. This article is an open access article distributed under the terms and conditions of the Creative Commons Attribution (CC BY) license (<https://creativecommons.org/licenses/by/4.0/>).

Keywords: ruthenium(II) complex; rhenium(I) complex; daminozide; apoptosis; anticancer

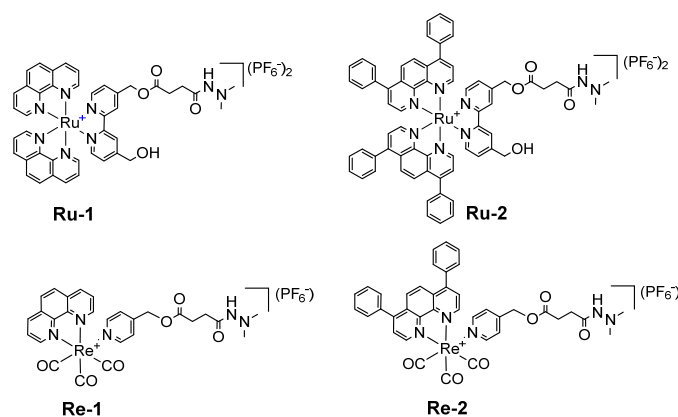
1. Introduction

Cancer is the archenemy of human health, and platinum-based drugs are one of the powerful weapons to fight against it [1,2]. Although cisplatin and its analogs have shown significant therapeutic efficacy in cancer treatment, their cytotoxic effects, including kidney toxicity, ototoxicity, neurotoxicity, etc. [3–5], highlight the pressing need to explore and develop a novel metal-based anticancer drug with reduced or negligible side effects to address the shortcomings of platinum-based drugs. Non-platinum group metals, such as rhenium [6–8], ruthenium [9,10], iridium [11–14], and gold [15,16], have been identified as potential anticancer agents. Compared with platinum-based drugs, ruthenium complexes exhibit lower toxicity and greater selectivity for tumor cells, rendering them a promising class of transition metal-based anticancer reagents. Rhenium complexes possess rich photochemical properties that can facilitate imaging [17], phototherapy [18,19], and radiotherapy [20]. Hence, the development of ruthenium(II) and rhenium(I) anticancer drugs presents the possibility to overcome the limitations of platinum-based drugs and provides greater opportunities for designing anticancer agents with optimal properties and functions.

Recently, more and more metal-based complexes are being used for the construction of enzyme inhibitors [21–24]. Jumonji domain-containing protein (JMJD) histone demethylases are important epigenetic regulators in cancer cells, which participate in the methylation of histone lysine residue 9 (H3K9) [25,26]. Various studies have shown that JMJD histone demethylases are overexpressed in various malignant tumors, which may

result in the downregulation of H3K9Me3 and the activation of oncogenes [27,28]. Thus, inhibition of JMJD can produce a substantial anti-tumor effect [29,30]. The research group led by Chung-Hang Leung designed and synthesized a Rh(III) complex, which has been identified as a selective and effective inhibitor of JMJD. It induces the accumulation of H3K4me3 and H3K4me2 levels in cells, leading to growth arrest in the G1 phase of triple-negative breast cancer [31]. Our group also reported two cases of metal-based complexes that can induce tumor cell death through JMJD inhibition [32,33].

Akane Kawamura's team found that the plant growth regulator daminozide selectively inhibited the JMJD ($IC_{50} = 1.5 \mu\text{M}$) [34]. In this study, daminozide was introduced into metal complexes to build multifunctional metal complexes. Four ruthenium(II)/rhenium(I)-daminozide conjugates (Scheme 1), with molecular formulas $[\text{Ru}(\text{N-N})_2\text{bpy}(4\text{-CH}_2\text{OH-4}'\text{-CH}_2\text{O-daminozide})](\text{PF}_6)_2$ (**Ru-1/Ru-2**) (N-N = 1,10-phenanthroline (phen, in **Ru-1**) and 4,7-diphenyl-1,10-phenanthroline (DIP, in **Ru-2**)) and $\text{Re}(\text{N-N})(\text{CO})_3(\text{PyCH}_2\text{O-daminozide})$ (**Re-1/Re-2**) (Py = pyridine, N-N = phen (in **Re-1**) and DIP (in **Re-2**)), are designed and synthesized. Moreover, the potential anticancer mechanisms of ruthenium(II)/rhenium(I)-daminozide conjugates were also elucidated, including JMJD inhibition, intracellular localization, mitochondrial function destruction, an increase of intracellular reactive oxygen species (ROS) level, promotion of cell apoptosis, and inhibition of cell migration and colony formation. In conclusion, these findings demonstrate the great potential of these metal complexes as anticancer agents.



Scheme 1. Chemical structures of Ru(II)/Re(I)-daminozide conjugates, **Ru-1/2** and **Re-1/2**.

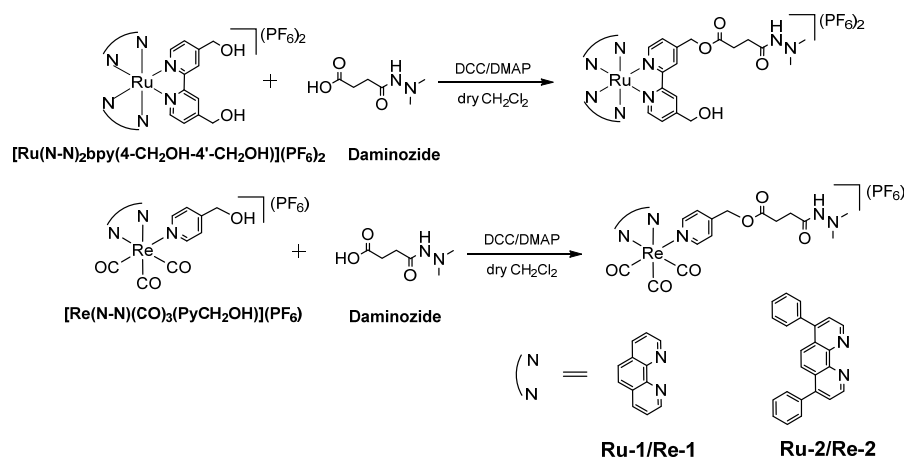
2. Results and Discussion

2.1. Synthesis, Photophysical Characterization

The synthetic route of Ru(II)/Re(I)-daminozide conjugates, **Ru-1/2** and **Re-1/2**, was shown in Scheme 2. Firstly, $[\text{Ru}(\text{phen})_2\text{bpy}(4\text{-CH}_2\text{OH-4}'\text{-CH}_2\text{OH})](\text{PF}_6)_2$ [35], $[\text{Ru}(\text{DIP})_2\text{bpy}(4\text{-CH}_2\text{OH-4}'\text{-CH}_2\text{OH})](\text{PF}_6)_2$ [35], $[\text{Re}(\text{phen})(\text{CO})_3(\text{PyCH}_2\text{OH})](\text{PF}_6)$ [36] and $[\text{Re}(\text{DIP})(\text{CO})_3(\text{PyCH}_2\text{OH})](\text{PF}_6)$ [36] were synthesized according to the references. Ru(II)/Re(I)-daminozide conjugates, **Ru-1/2** and **Re-1/2**, were then prepared through the condensation reaction of $[\text{Ru}(\text{N-N})_2\text{bpy}(4\text{-CH}_2\text{OH-4}'\text{-CH}_2\text{OH})](\text{PF}_6)_2$ / $[\text{Re}(\text{N-N})(\text{CO})_3(\text{PyCH}_2\text{OH})](\text{PF}_6)$ with daminozide in anhydrous CH_2Cl_2 at room temperature, with the aid of the dehydrating agent dicyclohexylcarbodiimide (DCC) and the catalyst 4-N,N-dimethylaminopyridine (DMAP). The products were purified using silica column chromatography, and their structures were confirmed by ^1H NMR, ^{31}P NMR, ESI-HRMS, and CHN elemental analysis (Figures S1–S12).

The electronic absorption and emission spectra of **Ru-1/2** and **Re-1/2** were shown in Figure S13. Both Ru(II) complexes and Re(I) complexes displayed 2 characteristic absorption bands at approximately 250–500 nm, which are classified as the intraligand and metal-to-ligand absorptions, respectively (Figure S13A). After excitation at 457 nm for Ru(II) and 405 nm for Re(I), **Ru-1/2** displayed orange luminescence with a maximum wavelength of around 600 nm (Figure S13B-a), and **Re-1/2** emitted green light with a

maximum wavelength of around 550 nm (Figure S13B-b). Their photophysical data are summarized in Table S1.



Scheme 2. Synthetic routes of **Ru-1/2** and **Re-1/2**.

2.2. Lipophilicity and In Vitro Cytotoxicity

The lipophilicity of a metal complex, as represented by its logarithmic partition coefficient ($\log P_{o/w}$), can potentially affect its cellular uptake, cytotoxicity, subcellular distribution, and anticancer mechanisms. The $\log P_{o/w}$ values of **Ru-1**, **Ru-2**, **Re-1**, and **Re-2** were determined by the shake-flask method and found to be **Re-2** (0.65) > **Ru-2** (0.57) > **Re-1** (−0.11) > **Ru-1** (−0.88). Subsequently, the antiproliferative activities of **Ru-1/2** and **Re-1/2** against different cell lines, including human cervical cancer cells (HeLa), human lung adenocarcinoma epithelial cells (A549), cisplatin-resistant A549 (A549R), human hepatocellular carcinoma (HepG2), and human normal liver cells (LO2), were evaluated using the 3-(4,5-dimethylthiazol-2-yl)-2,5-diphenyltetrazolium bromide (MTT) assay. Based on the IC_{50} values in Table 1, the antiproliferative effects of these compounds were as follows: **Ru-1**, **Re-1** < cisplatin < **Ru-2** < **Re-2**. **Re-2** was the most effective of all tested compounds, with an IC_{50} value range of around 2.0. **Ru-2** and **Re-2** all showed higher cytotoxic effects on HeLa cells than other cancer cell lines.

Table 1. IC_{50} values of tested compounds towards different cell lines ^a.

Compound	IC_{50} (μM)				
	HeLa	A549	A549R	HepG2	LO2
Ru-1	>50	>50	>50	>50	>50
Ru-2	5.0 ± 0.3	10.1 ± 2.2	12.3 ± 0.6	14.4 ± 1.6	18.2 ± 2.7
Re-1	>50	>50	>50	>50	>50
Re-2	2.0 ± 0.2	3.8 ± 1.1	2.6 ± 0.2	3.6 ± 0.3	7.6 ± 2.1
Cisplatin	26.1 ± 3.7	27.3 ± 6.1	>50	33.4 ± 4.3	35.5 ± 5.8

^a Cell viability is assessed after 48 h incubation. Data are presented as mean \pm standard deviation (SD).

2.3. Upregulation of the Histone-Methylation Level

The JMJD histone demethylase is overexpressed in various malignant tumors, which may result in the downregulation of H3K9Me3 and the activation of oncogenes [27,28]. The expression level of H3K9Me3 can be used as an alternative marker to monitor JMJD histone demethylase activity. In this study, we evaluated whether **Ru-2** and **Re-2** could alter the level of histone methylation. We examined the expression of H3K9Me3 by Western blot. As shown in Figure 1, both **Ru-2** and **Re-2** increased the expression of H3K9Me3 in a dose-dependent manner, indicating that JMJD activity is inhibited. It is worth noting that the reference complexes ($[\text{Ru}(\text{DIP})_2\text{bpy}(4\text{-CH}_2\text{OH-4}'\text{-CH}_2\text{OH})](\text{PF}_6)_2$ and $[\text{Re}(\text{DIP})(\text{CO})_3(\text{PyCH}_2\text{OH})](\text{PF}_6)$) did not show any inhibition effect, which further

showed that the inhibition of **Ru-2** and **Re-2** on JMJD was attributed to the introduction of daminozide.

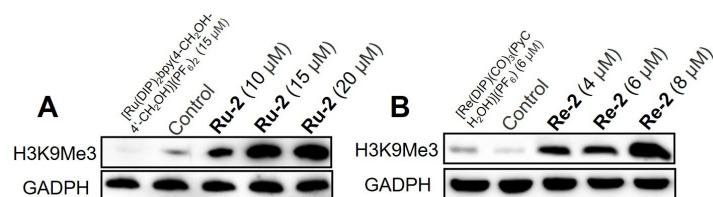


Figure 1. Dose-dependent effects of **Ru-2** (A) and **Re-2** (B) on H3K9Me3 after 24 h of treatment.

2.4. Cellular Localization and Uptake Mechanisms

Ru-2 and **Re-2** have been selected as target compounds due to their superior cytotoxicity and are being investigated for their anticancer mechanisms. These complexes exhibit luminescent properties, so it is easy to observe the distribution of **Ru-2** and **Re-2** in HeLa cells by confocal laser scanning microscope. We first studied the effect of HeLa cells pretreated with the metabolic inhibitor carbonyl cyanide m-chlorophenyl hydrazone (CCCP)/endocytic inhibitor chloroquine and incubated at 37 °C/4 °C on the uptake of **Ru-2** and **Re-2**. After pretreatment with metabolic inhibitor CCCP, HeLa cells were incubated with **Ru-2** and **Re-2**, resulting in weaker intracellular luminescence than at 37 °C (Figures 2A and S14). However, in the cells pretreated with the endocytosis inhibitor chloroquine, there was no significant change in the intracellular luminescence level of **Ru-2** and **Re-2**. The results indicate that **Ru-2** and **Re-2** are primarily absorbed by HeLa cells via an energy-dependent mechanism rather than an endocytic pathway. We further explored the subcellular localization of **Re-2** by co-staining HeLa cells with MTDR or LTDR and **Re-2**. As shown in Figure 2B, the luminescence of **Re-2** highly overlapped with the fluorescence of MTDR but almost no overlap with that of LTDR. These results indicate that **Re-2** localizes to mitochondria rather than lysosomes.

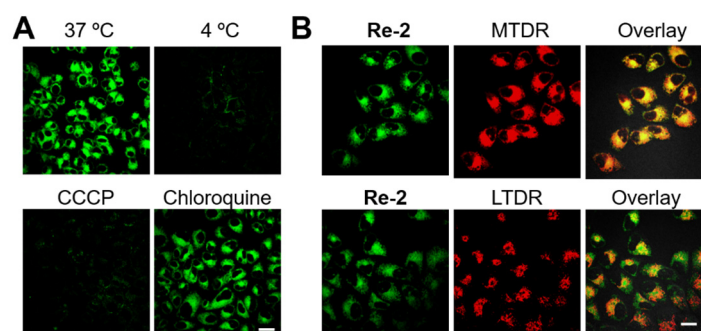


Figure 2. (A) Cellular uptake mechanisms of **Re-2**. HeLa cells were incubated with **Re-2** (10 μM, 1 h) under different conditions (37 °C, 4 °C, pre-treated HeLa cells with CCCP (30 μM) or chloroquine (50 μM)). (B) Confocal microscopic images of HeLa cells co-labeled with **Re-2** (10 μM, 1 h) and LTDR (50 nM, 0.5 h) or MTDR (150 nM, 0.5 h) ($\lambda_{\text{ex}} = 405 \text{ nm}$ for **Re-2** and 633 nm for MTDR/LTDR; $\lambda_{\text{em}} = 550 \pm 20 \text{ nm}$ for **Re-2** and 665 \pm 20 nm for MTDR/LTDR). Scale bar: 20 μm.

2.5. Mitochondrial Damage

Typically, mitochondria-targeted drugs can cause a series of mitochondrial damage, including a decrease in mitochondrial membrane potential (MMP) and an increase in ROS. 5,5',6,6'-Tetrachloro-1,1',3,3'-tetraethylbenzimidazolylcarbocyanine iodide (JC-1) is commonly used to evaluate the change of MMP through monitoring the ratio of red-to-green fluorescence intensity [37]. In control group cells, JC-1 mainly exists in the form of aggregates and displays red fluorescence. However, when MMP decreases, the monomer form of JC-1 increases, resulting in an increase in green fluorescence. As shown in Figure 3A,B, HeLa cells treated with different concentrations of **Ru-2** or **Re-2** showed a significant decrease in red fluorescence and an increase in green fluorescence as observed by confocal

microscopy, indicating the loss of MMP. The same phenomenon was also observed by flow cytometry (Figure 3C,D). The quantitative data of the ratio of green/red fluorescence intensity, as shown in Figure S15, compared with the control group, and **Ru-2**/**Re-2**-treated groups exhibited an increase in the ratio of green/red fluorescence intensity, with values of 1.1 (**Ru-2**, 10 μM), 1.8 (**Ru-2**, 15 μM), 2.1 (**Ru-2**, 20 μM), and 1.8 (**Re-2**, 4 μM), 2.6 (**Re-2**, 6 μM), and 3.9 (**Re-2**, 8 μM). These results indicate that these two complexes can reduce the MMP of HeLa cells in a concentration-dependent manner.

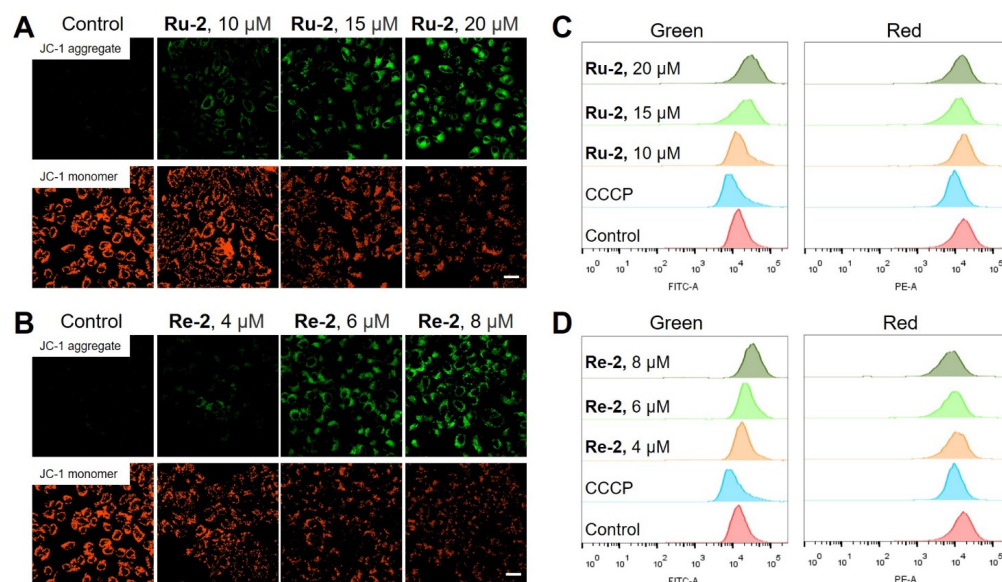


Figure 3. The loss of MMP examined by confocal microscope (A,B) and flow cytometry (C,D) with JC-1 staining after treatment with **Ru-2** and **Re-2** for 6 h ($\lambda_{\text{ex}} = 488 \text{ nm}$, $\lambda_{\text{em}} = 530 \pm 20 \text{ nm}$ for JC-1 monomer (green) and $585 \pm 20 \text{ nm}$ for JC-1 aggregates (red)). Scale bar: 20 μm .

2.6. Elevation of Intracellular ROS Levels

ROS are natural byproducts of normal oxygen metabolism, but excessive production of ROS within cells will disrupt mitochondrial integrity and induce apoptosis [38]. To investigate the effect of **Ru-2** and **Re-2** on ROS levels, the fluorescence probe 2',7'-dichlorofluorescein diacetate (H_2DCFDA) was used to observe ROS production in HeLa cells. H_2DCFDA is non-fluorescent and can be converted to highly fluorescent 2',7'-dichlorofluorescein (DCF) through the oxidation reaction of ROS in cells [39]. As shown in Figure 4A,B, treatment of HeLa cells with different concentrations of **Ru-2** and **Re-2** for 6 h resulted in a dose-dependent increase in ROS levels compared to the control group. In addition, the results of quantitative analysis of intracellular ROS by flow cytometry (Figures 4C and S16) showed that compared with the control group, the cells treated with **Ru-2** and **Re-2** showed an increase in mean fluorescence intensity (MFI), which were 2.9-fold (**Ru-2**, 10 μM), 4.8-fold (**Ru-2**, 15 μM), 8.3-fold (**Ru-2**, 20 μM), as well as 2.1-fold (**Re-2**, 4 μM), 2.4-fold (**Re-2**, 6 μM), and 2.6-fold (**Re-2**, 8 μM).

2.7. Induction of Apoptosis

To investigate the ability of **Ru-2** and **Re-2** to induce apoptosis, we used the fluorescent dye Hoechst 33342 to stain HeLa cells. As shown in Figure 5A,B, compared with the control group, **Ru-2**/**Re-2** treated groups exhibited typical morphological changes of apoptosis, including cell shrinkage and nuclear fragmentation, and this trend of change increased in a dose-dependent manner.

The externalization of phosphatidylserine (PS) is a typical marker of early cell apoptosis [40]. The apoptosis induced by **Ru-2** and **Re-2** was further verified by annexin V-labeled flow cytometry. As shown in Figure 5C, compared to the control group (11.3%), the cells treated with different concentrations of **Ru-2** and **Re-2** exhibited an increase in apop-

otic cells, with a percentage of 17.3% (**Ru-2**, 10 μM), 38.9% (**Ru-2**, 15 μM), 48.7% (**Ru-2**, 20 μM), 36.6% (**Re-2**, 4 μM), 53.7% (**Re-2**, 6 μM), and 76.3% (**Re-2**, 8 μM), respectively. These results indicate that the percentage of apoptotic cells increases in a concentration-dependent manner.

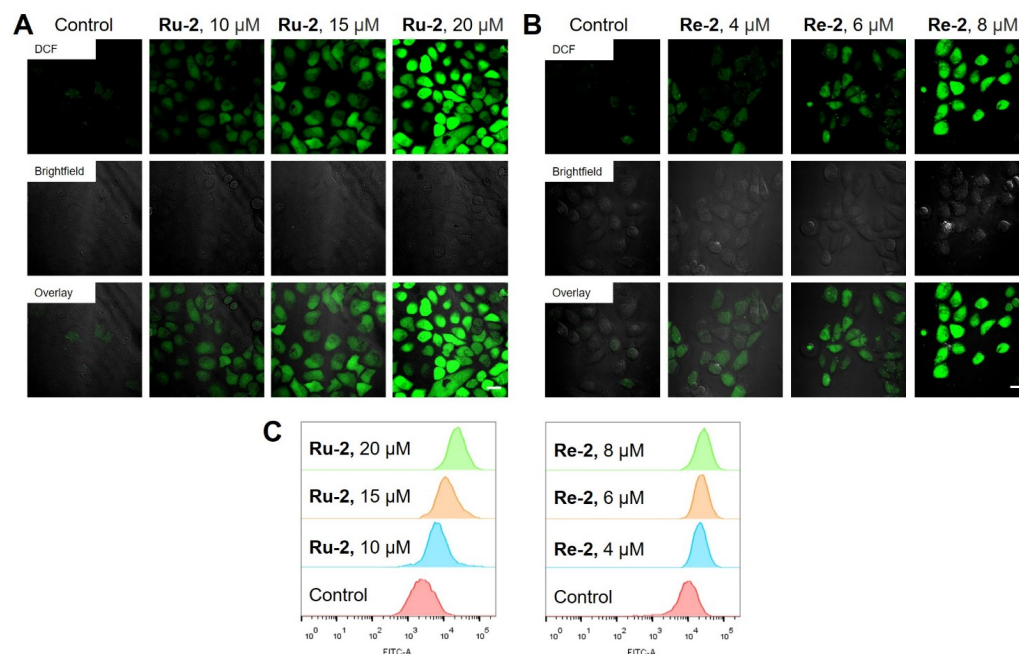


Figure 4. The elevation of intracellular ROS levels examined by confocal microscope (A,B) and flow cytometry (C) with H_2DCFDA staining after treatment with **Ru-2** and **Re-2** for 6 h ($\lambda_{\text{ex}} = 488 \text{ nm}$, $\lambda_{\text{em}} = 530 \pm 20 \text{ nm}$). Scale bar: 20 μm .

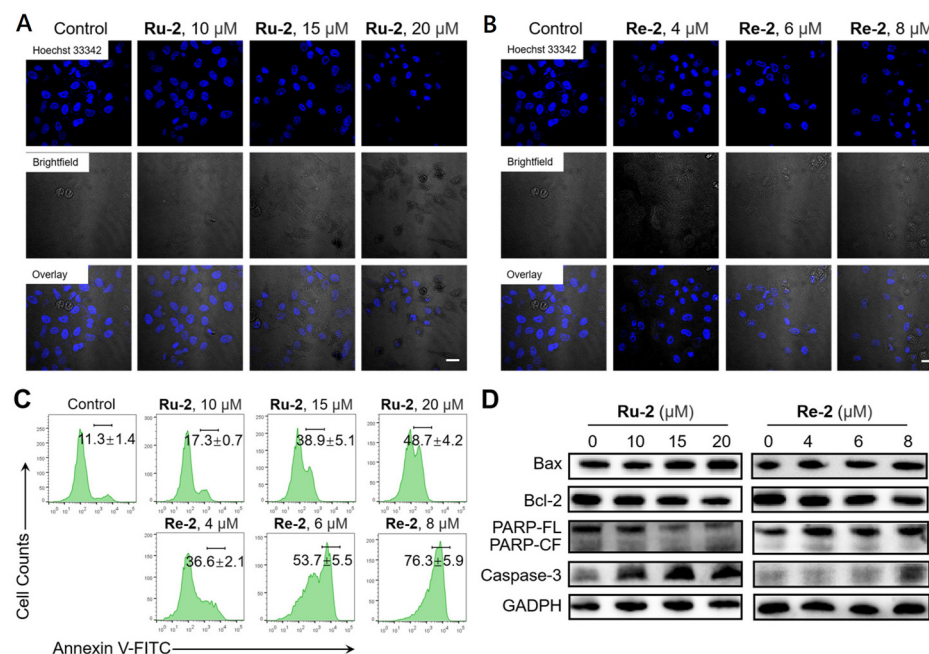


Figure 5. (A,B) Hoechst 33342 staining for the nuclei ($\lambda_{\text{ex}} = 405 \text{ nm}$, $\lambda_{\text{em}} = 460 \pm 20 \text{ nm}$). Scale bar: 20 μm . (C) Flow-cytometric quantification of Annexin V-labeled cells after treatment with **Ru-2** and **Re-2** for 24 h. (D) Western blot analysis of apoptosis-related protein (Bax, Bcl-2, PARP, and Caspase-3) in HeLa cells treated with **Ru-2** and **Re-2** for 24 h.

To further investigate the apoptotic mechanism induced by **Ru-2** and **Re-2**, we examined the expression of several relevant proteins, including caspase-3, poly (ADP-ribose)

polymerase (PARP), B-cell lymphoma-2 (Bcl-2), and Bcl-2-associated X protein (Bax). Caspase-3 and PARP are important biomarkers of apoptosis, and caspase-3 is a direct participant in the process [41]. Bax is involved in the mitochondrial-related caspase activation pathway, while Bcl-2 can inhibit the action of caspase-3 [42]. As shown in Figure 5D, **Ru-2** and **Re-2** upregulated the expression of Bax and caspase-3, downregulated the expression of Bcl-2, and induced the cleavage of PARP. These results suggest that **Ru-2** and **Re-2** can induce apoptosis through a caspase-dependent pathway.

2.8. Inhibition of Cell Migration and Colony Formation

Cell migration and invasion assays are common experimental technologies in the field of cancer research. The main purpose of these tests is to evaluate the migration and invasion abilities of cancer cells. As shown in the wound healing assay (Figure 6A,B), significant migration inhibition was observed in cells treated with **Ru-2** and **Re-2** at 24 and 48 h, demonstrating a concentration-dependent effect. After incubation for 48 h, the wound closure rate was 17.2% in cells treated with **Ru-2** (15 μM) and 6.3% in cells treated with **Re-2** (4 μM), far lower than that of the control group (69.8%). Additionally, the colony formation assay (Figure 6C,D) revealed that **Ru-2** and **Re-2** had good anti-proliferative activity. These results demonstrate that these two compounds have a significant inhibitory effect on the migration ability of cancer cells.

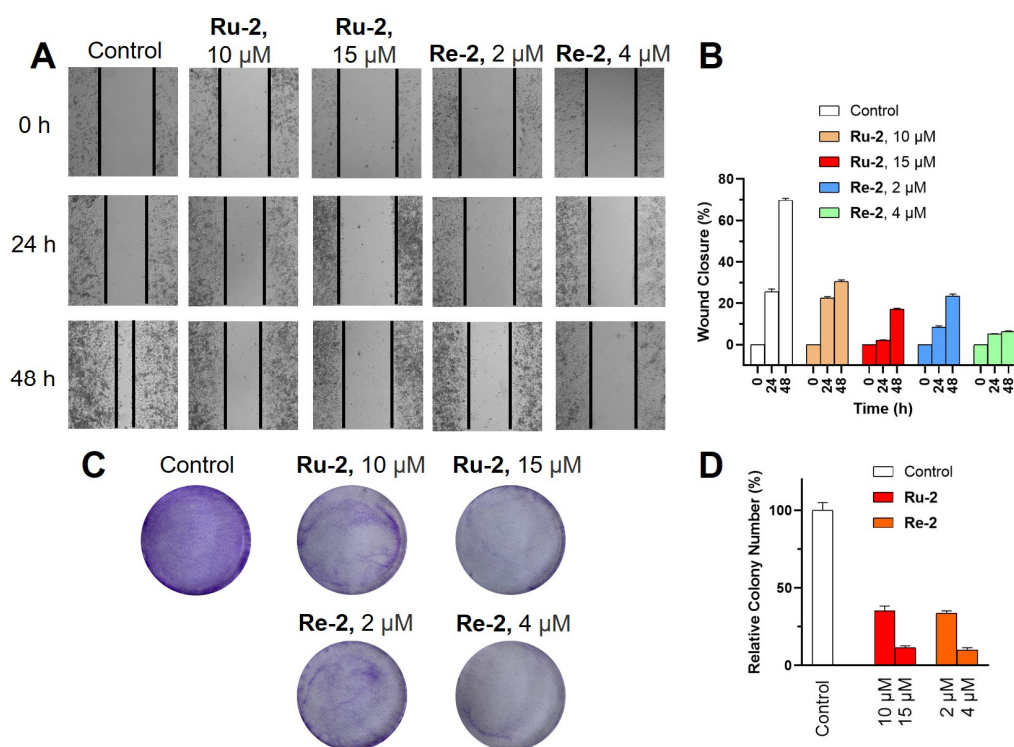


Figure 6. (A) Representative images of wound healing assay after treatment with **Ru-2** and **Re-2** for 0 h, 24 h, and 48 h. (B) Quantitative data of wound healing. Wound closure (%) = $[1 - (\text{width at indicated time})/(\text{width at 0 h})] \times 100\%$. (C) Images of colony formation after treatment with **Ru-2** and **Re-2**. (D) Quantitative data of colony formation assays.

3. Materials and Methods

3.1. Materials and Instruments

$\text{RuCl}_3 \cdot n\text{H}_2\text{O}$ (J&K, Beijing, China), $\text{Re}(\text{CO})_5\text{Cl}$ (J&K, Beijing, China), phen (J&K, Beijing, China), DIP (J&K, Beijing, China), daminozide (Alfa Aesar, Haverhill, MA, USA), DMAP (Alfa Aesar, Haverhill, MA, USA), DCC (Alfa Aesar, Haverhill, MA, USA), MTT (J&K, Beijing, China), CCCP (J&K, Beijing, China), chloroquine (J&K, Beijing, China), MTDR (Life Technologies, Carlsbad, CA, USA), LTDR (Life Technologies, Carlsbad, CA, USA),

H₂DCFDA (J&K, Beijing, China), JC-1 (Beyotime Biotechnology, Shanghai, China), Hoechst 33342 (J&K, Beijing, China), Annexin V-FITC Apoptosis Detection Kit (Beyotime Biotechnology, Shanghai, China). Primary antibodies against Bax, Bcl-2, caspase-3, PARP, and H3K9Me3 were obtained from Cell Signaling Technology.

ESI-HRMS spectra were obtained with an Agilent 6500 LC/Q-TOF mass spectrometer. ¹H NMR spectra were recorded on a Bruker Avance 600 spectrometer. Cell viability was measured with a SpetraMax M2 plate reader. Cell imaging was carried out using a Nikon A1R/A1 laser-scanning confocal microscope, and flow cytometry was conducted on a BD FACSAria flow cytometer.

3.2. Preparation of Ruthenium(II) and Rhenium(I) Complexes

[Ru(phen)₂bpy(4-CH₂OH-4'-CH₂OH)](PF₆)₂ [35], [Ru(DIP)₂bpy(4-CH₂OH-4'-CH₂OH)](PF₆)₂ [35], [Re(phen)(CO)₃(PyCH₂OH)](PF₆) [36] and [Re(DIP)(CO)₃(PyCH₂OH)](PF₆) [36] were synthesized following the literature procedures.

[Ru(phen)₂((4'-(hydroxymethyl)-[2,2'-bipyridin]-4-yl)methyl 4-(2,2-dimethylhydrazineyl)-4-oxobutanoate)](PF₆)₂ **Ru-1**: The synthetic route of **Ru-1** was shown in Scheme 2. After stirring the mixture of daminozide (5 equiv.), DMAP (1.5 equiv.), and DCC (1.5 equiv.) in dry CH₂Cl₂ for 30 min, [Ru(phen)₂bpy(4-CH₂OH-4'-CH₂OH)](PF₆)₂ (1 equiv.) in dry CH₂Cl₂ was added drop-wise and stirred at ambient temperature for 24 h. Then, the solvent was evaporated, and the crude product was purified using column chromatography on silica gel by elution with acetonitrile/water/saturated potassium nitrate (100:9:1, *v/v/v*). Yield: 0.185 g (orange powder), 72%. ¹H NMR (600 MHz, [D₆]DMSO) δ 9.00 (d, *J* = 17.2 Hz, 1H), 8.86–8.80 (m, 3H), 8.74 (d, *J* = 7.9 Hz, 2H), 8.46–8.32 (m, 5H), 8.28–8.25 (m, 2H), 7.96 (m, 4H), 7.72 (dd, *J* = 8.0, 5.4 Hz, 2H), 7.66–7.62 (m, 2H), 7.39–7.33 (m, 2H), 5.79 (q, *J* = 5.7 Hz, 1H), 5.35 (d, *J* = 9.2 Hz, 2H), 4.77 (dd, *J* = 16.5, 5.2 Hz, 2H), 2.65 (ddd, *J* = 21.5, 14.0, 6.7 Hz, 3H), 2.42 (s, 3H), 2.35 (s, 4H). ³¹P NMR (161.98 MHz, [D₆]DMSO) δ -133.65, -137.17, -140.68, -144.19, -147.70, -151.21, -154.73. ESI-HRMS (CH₃OH): *m/z* 965.1701 [M-PF₆]⁺, 882.1934 [M-2PF₆-H + 2CH₃OH]⁺, 410.1031 [M-2PF₆]²⁺. Elemental analysis: calcd (%) for C₄₂H₃₈F₁₂N₈O₄P₂Ru: C, 45.45; H, 3.45; N, 10.10; found: C, 45.58; H, 3.40; N, 10.30.

[Ru(DIP)₂((4'-(hydroxymethyl)-[2,2'-bipyridin]-4-yl)methyl 4-(2,2-dimethylhydrazineyl)-4-oxobutanoate)](PF₆)₂ **Ru-2**: **Ru-2** was prepared following a similar procedure to that of **Ru-1**, except [Ru(DIP)₂bpy(4-CH₂OH-4'-CH₂OH)](PF₆)₂ was used instead of [Ru(phen)₂bpy(4-CH₂OH-4'-CH₂OH)](PF₆)₂. Yield: 0.167 g (orange powder), 77%. ¹H NMR (600 MHz, [D₆]DMSO) δ 9.03 (d, *J* = 46.8 Hz, 1H), 8.90–8.80 (m, 1H), 8.38–8.34 (m, 2H), 8.31–8.21 (m, 6H), 7.99–7.91 (m, 2H), 7.83–7.59 (m, 25H), 7.50–7.43 (m, 2H), 5.85 (q, *J* = 5.3, 3.8 Hz, 1H), 5.40 (d, *J* = 9.4 Hz, 2H), 4.82 (dd, *J* = 15.7, 4.7 Hz, 2H), 2.66 (ddd, *J* = 17.2, 11.1, 6.6 Hz, 3H), 2.40 (s, 3H), 2.36 (s, 4H). ³¹P NMR (161.98 MHz, [D₆]DMSO) δ -133.67, -137.18, -140.66, -144.18, -147.71, -151.23, -154.74. ESI-HRMS (CH₃OH): *m/z* 1269.2964 [M-PF₆]⁺, 562.1662 [M-2PF₆]²⁺. Elemental analysis: calcd (%) for C₆₆H₅₄F₁₂N₈O₄P₂Ru: C, 56.05; H, 3.85; N, 7.92; found: C, 56.36; H, 3.60; N, 8.02.

[Re(phen)(pyridin-4-ylmethyl 4-(2,2-dimethylhydrazineyl)-4-oxobutanoate)](PF₆) **Re-1**: **Re-1** was prepared following a similar procedure to that of **Ru-1**, except [Re(phen)(CO)₃(PyCH₂OH)](PF₆) was used instead of [Ru(phen)₂bpy(4-CH₂OH-4'-CH₂OH)](PF₆)₂. The crude product was purified using column chromatography on silica gel by elution with CH₂Cl₂/CH₃OH (10:1, *v/v*). Yield: 0.180 g (light yellow powder), 75%. ¹H NMR (600 MHz, [D₆]DMSO) δ 9.78 (t, *J* = 4.6 Hz, 2H), 9.05 (d, *J* = 8.2 Hz, 2H), 8.77 (s, 1H), 8.43 (d, *J* = 5.8 Hz, 2H), 8.32 (s, 2H), 8.26 (dd, *J* = 8.1, 5.2 Hz, 2H), 7.27 (d, *J* = 5.5 Hz, 2H), 5.01 (s, 2H), 4.39 (s, 2H), 2.56 (t, *J* = 6.2 Hz, 1H), 2.35 (d, *J* = 21.4 Hz, 6H), 2.19 (t, *J* = 6.6 Hz, 1H). ³¹P NMR (161.98 MHz, [D₆]DMSO) δ -133.65, -137.16, -140.67, -144.19, -147.70, -151.21, -154.72. ESI-HRMS (CH₃OH): *m/z* 702.1352 [M-PF₆]⁺, 451.0099 [Re(phen)(CO)₃]⁺, 252.1342 [M-PF₆-Re(phen)(CO)₃ + H]⁺. Elemental analysis: calcd (%) for C₂₇H₂₅F₆N₅O₆Pre: C, 38.30; H, 2.98; N, 8.27; found: C, 38.45; H, 2.78; N, 8.50.

[Re(DIP)(pyridin-4-ylmethyl 4-(2,2-dimethylhydrazineyl)-4-oxobutanoate)](PF₆) **Re-2**: **Re-2** was prepared following a similar procedure to that of **Re-1**, except [Re(DIP)(CO)₃(PyCH₂OH)](PF₆) was used instead of [Re(phen)(CO)₃(PyCH₂OH)](PF₆). Yield: 0.158 g (yellow powder), 70%. ¹H NMR (600 MHz, [D₆]DMSO) δ 9.84 (t, *J* = 5.4 Hz, 2H), 8.79 (s, 1H), 8.59 (d, *J* = 6.3 Hz, 2H), 8.22 (d, *J* = 5.3 Hz, 2H), 8.16 (s, 2H), 7.70 (m, 10H), 7.37 (d, *J* = 5.5 Hz, 2H), 5.08 (s, 2H), 2.58 (t, *J* = 6.3 Hz, 1H), 2.53 (m, 2H), 2.35 (d, *J* = 17.8 Hz, 6H), 2.21 (t, *J* = 6.6 Hz, 1H). ³¹P NMR (161.98 MHz, [D₆]DMSO) δ −133.65, −137.17, −140.68, −144.19, −147.70, −151.22, −154.73. ESI-HRMS (CH₃OH): *m/z* 854.1980 [M-PF₆]⁺, 603.0718 [Re(DIP)(CO)₃]⁺, 252.1341 [M-PF₆-Re(DIP)(CO)₃+ H]⁺. Elemental analysis: calcd (%) for C₃₉H₃₃F₆N₅O₆Pre: C, 46.89; H, 3.33; N, 7.01; found: C, 46.93; H, 3.25; N, 7.33.

3.3. Cell Lines and Culture Conditions

HeLa, HepG2, A549, A549R, and LO2 cells were purchased from Nanjing KeyGen Biotechnology Co., Ltd., and cultured in DMEM or RPMI 1640 complete medium at 37 °C with 5% CO₂ atmosphere.

3.4. In Vitro Cytotoxicity Assay

The anti-cancer effects of ruthenium(II) and rhenium(I) complexes against HeLa, A549, A549R, HepG2, and LO2 cell lines were evaluated by MTT method. Cells were seeded at a density of 5 × 10⁴/well in 96-well plates and incubated at 37 °C for 24 h. Afterward, the culture medium was replaced with fresh medium containing the ruthenium(II) and rhenium(I) complexes, and the cells were further incubated at 37 °C for 48 h. MTT solution was added, and the cells were co-incubated at 37 °C for an additional 4 h. Finally, 150 μL/well DMSO was added to dissolve the MTT-formazan crystals, and the absorbance of living cells at 570 nm was measured using a SpetraMax M2 plate reader.

3.5. Cellular Localization Assay

HeLa cells were cultured in confocal dishes for 24 h. Next, a solution of **Re-2** (10 μM) was added and incubated for 30 min. After that, commercial lysosomal probe LTDR (50 nM) or mitochondrial probe MTDR (150 nM) was added to incubate the cells for another 30 min. Subsequently, cells were washed with PBS and visualized using confocal microscopy. **Re-2** and LTDR/MTDR were excited at 405 nm and 633 nm, respectively. The emission wavelengths of **Re-2** and LTDR/MTDR were 550 ± 20 nm and 665 ± 20 nm, respectively.

3.6. Measurement of MMP

HeLa cells were seeded into confocal dishes and cultured for 24 h. After incubation with **Ru-2** or **Re-2** for 6 h, cells were washed twice with PBS and stained with JC-1 (5 μg/mL) for 30 min. After that, cells were analyzed by confocal microscopy or flow cytometry. The excitation wavelength of JC-1 was 488 nm, the emission wavelength was 530 ± 20 nm for JC-1 monomer (green), and 585 ± 20 nm for JC-1 aggregate (red).

3.7. Measurement of Intracellular ROS

After 6 h of treatment with **Ru-2** or **Re-2**, cells were stained with H₂DCFDA for 25 min at 37 °C. Subsequently, cells were washed three times with serum-free DMEM. The fluorescence intensity of DCF was measured by confocal laser scanning microscopy and flow cytometry (λ_{ex} = 488 nm; λ_{em} = 530 ± 20 nm).

3.8. Hoechst 33342 Staining

After treatment with the indicated concentrations of **Ru-2** or **Re-2** for 24 h, cells were fixed with 4% paraformaldehyde for 15 min, followed by staining with Hoechst 33342 (5 μg/mL). Finally, the morphology of cell nuclei was visualized under a confocal microscope (λ_{ex} = 405 nm; λ_{em} = 460 ± 20 nm).

3.9. Annexin V Staining

After 24 h of treatment with **Ru-2** or **Re-2** at the indicated concentrations, cells were re-suspended with Annexin-binding buffer (195 μ L) and labelled with Annexin V (5 μ L). The samples were analyzed by flow cytometry ($\lambda_{\text{ex}} = 488 \text{ nm}$; $\lambda_{\text{em}} = 530 \pm 20 \text{ nm}$).

3.10. Wound Healing Assay

HeLa cells were seeded into a 6-well plate. After reaching 85% confluency, a sterile 200 μ L pipette tip was used to make cross-shaped scratches in the center of each well, and excess cells were carefully washed away with DMEM medium. Then, cells were further cultured in medium containing **Ru-2** or **Re-2**. The closure of the wounds was monitored and imaged at 0 h, 24 h, and 48 h using an inverted microscope.

3.11. Statistical Analysis

The biological experiments were conducted at least 3 repetitions, and the data were reported as means \pm SD.

4. Conclusions

In conclusion, we have designed and synthesized four Ru(II)/Re(I)-daminozide conjugates, **Ru-1/2** and **Re-1/2**. MTT assay results showed that **Ru-2** and **Re-2** had a highly cytotoxic effect on human tumor cells. Further research revealed that **Ru-2** and **Re-2** could inhibit the activity of JMJD histone demethylase, lead to the depolarization of the mitochondrial membrane, an increase in ROS levels, and induction of HeLa cell apoptosis via the caspase cascade pathway. These compounds can achieve multiple therapeutic effects (among them, daminozide fragment is more responsible for the inhibition of the activity of JMJD histone demethylase, and metal centers are more responsible for the localization of mitochondria and the induction of mitochondrial damage) and have great potential for developing anti-cancer drugs. Therefore, our study suggests that combining JMJD inhibitors with metal complexes is an effective strategy for developing new tumor-targeted and multifunctional metal anti-cancer drugs.

Supplementary Materials: The following supporting information can be downloaded at: <https://www.mdpi.com/article/10.3390/inorganics11040142/s1>, Figure S1: ESI-HRMS characterization of **Ru-1**; Figure S2: ESI-HRMS characterization of **Ru-2**; Figure S3: ESI-HRMS characterization of **Re-1**; Figure S4: ESI-HRMS characterization of **Re-2**; Figure S5: ^1H NMR spectrum of **Ru-1**; Figure S6: ^1H NMR spectrum of **Ru-2**; Figure S7: ^1H NMR spectrum of **Re-1**; Figure S8: ^1H NMR spectrum of **Re-2**; Figure S9: ^{31}P NMR spectrum of **Ru-1**; Figure S10: ^{31}P NMR spectrum of **Ru-2**; Figure S11: ^{31}P NMR spectrum of **Re-1**; Figure S12: ^{31}P NMR spectrum of **Re-2**; Figure S13: UV/Vis and emission spectra of Ru(II) and Re(I) complexes; Figure S14: Cellular uptake mechanisms of **Ru-2**; Figure S15: Ratio of green to red fluorescence intensity; Figure S16: Quantitative data of MFI; Table S1: Photophysical data of Ru(II) and Re(I) complexes.

Author Contributions: P.-X.Y. and M.-R.C.: contributed to the synthesis and characterization of complexes and wrote the article. K.X. and Z.Z.: studied the anti-tumor mechanism and wrote the article. B.H., R.-T.L. and R.-R.Y.: provided the methodology and wrote and revised the article. All authors have read and agreed to the published version of the manuscript.

Funding: This research was funded by the National Natural Science Foundation of China (21967014, 22007042), Applied Basic Research Projects of Yunnan Province (202001AT070036), High-level Scientific Research Foundation for Talent Introduction of Kunming University of Science and Technology (KKKP201826008).

Data Availability Statement: All data is available in this manuscript or the Supporting Information.

Conflicts of Interest: The authors declare no conflict of interest.

References

1. Ludwig, H.; Novis Durie, S.; Meckl, A.; Hinke, A.; Durie, B. Multiple Myeloma Incidence and Mortality around the Globe; Interrelations between Health Access and Quality, Economic Resources, and Patient Empowerment. *Oncologist* **2020**, *25*, e1406–e1413. [[CrossRef](#)] [[PubMed](#)]
2. Rashedi, A.S.; De Roo, S.F.; Ataman, L.M.; Edmonds, M.E.; Silva, A.A.; Scarella, A.; Horbaczewska, A.; Anazodo, A.; Arvas, A.; Ramalho de Carvalho, B. Survey of Fertility Preservation Options Available to Patients with Cancer around the Globe. *JCO Glob. Oncol.* **2020**, *6*, 331–344. [[CrossRef](#)] [[PubMed](#)]
3. Dilruba, S.; Kalayda, G.V. Platinum-Based Drugs: Past, Present and Future. *Cancer Chemother. Pharmacol.* **2016**, *77*, 1103–1124. [[CrossRef](#)]
4. Oun, R.; Moussa, Y.E.; Wheate, N.J. The Side Effects of Platinum-Based Chemotherapy Drugs: A Review for Chemists. *Dalton Trans.* **2018**, *47*, 6645–6653. [[CrossRef](#)]
5. Yin, J.-Y.; Li, X.; Li, X.-P.; Xiao, L.; Zheng, W.; Chen, J.; Mao, C.-X.; Fang, C.; Cui, J.-J.; Guo, C.-X. Prediction Models for Platinum-Based Chemotherapy Response and Toxicity in Advanced NSCLC Patients. *Cancer Lett.* **2016**, *377*, 65–73. [[CrossRef](#)] [[PubMed](#)]
6. Leonidova, A.; Gasser, G. Underestimated Potential of Organometallic Rhenium Complexes as Anticancer Agents. *ACS Chem. Biol.* **2014**, *9*, 2180–2193. [[CrossRef](#)] [[PubMed](#)]
7. He, S.-F.; Liao, J.-X.; Huang, M.-Y.; Zhang, Y.-Q.; Zou, Y.-M.; Wu, C.-L.; Lin, W.-Y.; Chen, J.-X.; Sun, J. Rhenium–Guanidine Complex as Photosensitizer: Trigger HeLa Cell Apoptosis through Death Receptor-Mediated, Mitochondria-Mediated, and Cell Cycle Arrest Pathways. *Metallomics* **2022**, *14*, mfac008. [[CrossRef](#)] [[PubMed](#)]
8. He, L.; Pan, Z.-Y.; Qin, W.-W.; Li, Y.; Tan, C.-P.; Mao, Z.-W. Impairment of the Autophagy-Related Lysosomal Degradation Pathway by an Anticancer Rhenium(I) Complex. *Dalton Trans.* **2019**, *48*, 4398–4404. [[CrossRef](#)] [[PubMed](#)]
9. Lee, L.C.-C.; Lo, K.K.-W. Strategic Design of Luminescent Rhenium(I), Ruthenium(II), and Iridium(III) Complexes as Activity-Based Probes for Bioimaging and Biosensing. *Chem. Asian J.* **2022**, *17*, e202200840. [[CrossRef](#)]
10. Olelewe, C.; Awuah, S.G. Mitochondria as a Target of Third Row Transition Metal-Based Anticancer Complexes. *Curr. Opin. Chem. Biol.* **2023**, *72*, 102235. [[CrossRef](#)]
11. Ye, R.-R.; Peng, W.; Chen, B.-C.; Jiang, N.; Chen, X.-Q.; Mao, Z.-W.; Li, R.-T. Mitochondria-Targeted Artesunate Conjugated Cyclometalated Iridium(III) Complexes as Potent Anti-HepG2 Hepatocellular Carcinoma Agents. *Metallomics* **2020**, *12*, 1131–1141. [[CrossRef](#)] [[PubMed](#)]
12. Lo, K.K.-W.; Zhang, K.Y. Iridium(III) Complexes as Therapeutic and Bioimaging Reagents for Cellular Applications. *RSC Adv.* **2012**, *2*, 12069–12083. [[CrossRef](#)]
13. Liu, Z.; Romero-Canelón, I.; Habtemariam, A.; Clarkson, G.J.; Sadler, P.J. Potent Half-Sandwich Iridium(III) Anticancer Complexes Containing CAN-Chelated and Pyridine Ligands. *Organometallics* **2014**, *33*, 5324–5333. [[CrossRef](#)] [[PubMed](#)]
14. Hearn, J.M.; Romero-Canelón, I.; Qamar, B.; Liu, Z.; Hands-Portman, I.; Sadler, P.J. Organometallic Iridium(III) Anticancer Complexes with New Mechanisms of Action: NCI-60 Screening, Mitochondrial Targeting, and Apoptosis. *ACS Chem. Biol.* **2013**, *8*, 1335–1343. [[CrossRef](#)]
15. Lu, Y.; Ma, X.; Chang, X.; Liang, Z.; Lv, L.; Shan, M.; Lu, Q.; Wen, Z.; Gust, R.; Liu, W. Recent Development of Gold(I) and Gold(III) Complexes as Therapeutic Agents for Cancer Diseases. *Chem. Soc. Rev.* **2022**, *51*, 5518–5556. [[CrossRef](#)]
16. Yang, Z.; Bian, M.; Lv, L.; Chang, X.; Wen, Z.; Li, F.; Lu, Y.; Liu, W. Tumor-Targeting NHC–Au(I) Complex Induces Immunogenic Cell Death in Hepatocellular Carcinoma. *J. Med. Chem.* **2023**, *66*, 3934–3952. [[CrossRef](#)]
17. Lee, L.C.-C.; Leung, K.-K.; Lo, K.K.-W. Recent Development of Luminescent Rhenium(I) Tricarbonyl Polypyridine Complexes as Cellular Imaging Reagents, Anticancer Drugs, and Antibacterial Agents. *Dalton Trans.* **2017**, *46*, 16357–16380. [[CrossRef](#)]
18. Wähler, K.; Ludewig, A.; Szabo, P.; Harms, K.; Meggers, E. Rhenium Complexes with Red-Light-Induced Anticancer Activity. *Eur. J. Med. Chem.* **2014**, *2014*, 807–811. [[CrossRef](#)]
19. Kastl, A.; Dieckmann, S.; Wähler, K.; Völker, T.; Kastl, L.; Merkel, A.L.; Vultur, A.; Shannan, B.; Harms, K.; Ocker, M. Rhenium Complexes with Visible-Light-Induced Anticancer Activity. *ChemMedChem* **2013**, *8*, 924–927. [[CrossRef](#)]
20. Martínez-Lillo, J.; Mastropietro, T.F.; Lappano, R.; Madeo, A.; Alberto, M.E.; Russo, N.; Maggiolini, M.; De Munno, G. Rhenium (IV) Compounds Inducing Apoptosis in Cancer Cells. *Chem. Commun.* **2011**, *47*, 5283–5285. [[CrossRef](#)]
21. Cheng, Y.; Qi, Y. Current Progresses in Metal-based Anticancer Complexes as Mammalian TrxR Inhibitors. *Anticancer Agents Med. Chem.* **2017**, *17*, 1046–1069. [[CrossRef](#)]
22. Ye, R.; Tan, C.; Chen, B.; Li, R.; Mao, Z. Zinc-Containing Metalloenzymes: Inhibition by Metal-Based Anticancer Agents. *Front. Chem.* **2020**, *8*, 402. [[CrossRef](#)] [[PubMed](#)]
23. Dörr, M.; Meggers, E. Metal complexes as structural templates for targeting proteins. *Curr. Opin. Chem. Biol.* **2014**, *19*, 76–81. [[CrossRef](#)] [[PubMed](#)]
24. He, L.; Xiong, K.; Wang, L.; Guan, R.; Chen, Y.; Ji, L.; Chao, H. Iridium(III) complexes as mitochondrial topoisomerase inhibitors against cisplatin-resistant cancer cells. *Chem. Commun.* **2021**, *57*, 8308–8311. [[CrossRef](#)]
25. Berry, W.L.; Janknecht, R. KDM4/JMJD2 histone demethylases: Epigenetic regulators in cancer cells. *Cancer Res.* **2013**, *73*, 2936–2942. [[CrossRef](#)] [[PubMed](#)]

26. Fan, L.; Xu, S.; Zhang, F.; Cui, X.; Fazli, L.; Gleave, M.; Clark, D.J.; Yang, A.; Hussain, A.; Rassool, F.; et al. Histone demethylase JMJD1A promotes expression of DNA repair factors and radio-resistance of prostate cancer cells. *Cell Death Dis.* **2020**, *11*, 214. [[CrossRef](#)]
27. Morera, L.; Lubbert, M.; Jung, M. Targeting histone methyl-transferases and demethylases in clinical trials for cancer therapy. *Clin. Epigenetics* **2016**, *8*, 57. [[CrossRef](#)]
28. Varier, R.A.; Timmers, H.T. Histone lysine methylation and demethylation pathways in cancer. *Biochim. Biophys. Acta* **2011**, *1815*, 75–89. [[CrossRef](#)]
29. Yang, G.J.; Wu, J.; Miao, L.; Zhu, M.H.; Zhou, Q.J.; Lu, X.J.; Lu, J.F.; Leung, C.H.; Ma, D.L.; Chen, J. Pharmacological inhibition of KDM5A for cancer treatment. *Eur. J. Med. Chem.* **2021**, *226*, 113855. [[CrossRef](#)]
30. Kaniskan, H.U.; Martini, M.L.; Jin, J. Inhibitors of protein methyltransferases and demethylases. *Chem. Rev.* **2018**, *118*, 989–1068. [[CrossRef](#)]
31. Yang, G.-J.; Wang, W.; Mok, S.W.F.; Wu, C.; Law, B.Y.K.; Miao, X.-M.; Wu, K.-J.; Zhong, H.-J.; Wong, C.-Y.; Wong, V.K.W. Selective Inhibition of Lysine-Specific Demethylase 5A (KDM5A) Using a Rhodium(III) Complex for Triple-Negative Breast Cancer Therapy. *Angew. Chem. Int. Ed.* **2018**, *130*, 13275–13279. [[CrossRef](#)]
32. Ma, X.; Lu, J.; Yang, P.; Zhang, Z.; Huang, B.; Li, R.; Ye, R. 8-Hydroxyquinoline-Modified Ruthenium(II) Polypyridyl Complexes for JMJD Inhibition and Photodynamic Antitumor Therapy. *Dalton Trans.* **2022**, *51*, 13902–13909. [[CrossRef](#)]
33. Lu, J.-J.; Ma, X.-R.; Xie, K.; Chen, M.-R.; Huang, B.; Li, R.-T.; Ye, R.-R. Lysosome-Targeted Cyclometalated Iridium(III) Complexes: JMJD Inhibition, Dual Induction of Apoptosis, and Autophagy. *Metallomics* **2022**, *14*, mfac068. [[CrossRef](#)]
34. Rose, N.R.; Woon, E.C.; Tumber, A.; Walport, L.J.; Chowdhury, R.; Li, X.S.; King, O.N.; Lejeune, C.; Ng, S.S.; Krojer, T. Plant Growth Regulator Daminozide Is a Selective Inhibitor of Human KDM2/7 Histone Demethylases. *J. Med. Chem.* **2012**, *55*, 6639–6643. [[CrossRef](#)]
35. Chen, B.-C.; Lu, J.-J.; Jiang, N.; Ma, X.-R.; Li, R.-T.; Ye, R.-R. Synthesis, characterization and antitumor mechanism investigation of ruthenium(II) polypyridyl complexes with artesunate moiety. *J. Biol. Inorg. Chem.* **2021**, *26*, 909–918. [[CrossRef](#)]
36. Ye, R.-R.; Chen, B.-C.; Lu, J.-J.; Ma, X.-R.; Li, R.-T. Phosphorescent Rhenium(I) Complexes Conjugated with Artesunate: Mitochondrial Targeting and Apoptosis-Ferroptosis Dual Induction. *J. Inorg. Biochem.* **2021**, *223*, 111537. [[CrossRef](#)] [[PubMed](#)]
37. Smiley, S.T.; Reers, M.; Mottola-Hartshorn, C.; Lin, M.; Chen, A.; Smith, T.W.; Steele, G.D.; Chen, L.B. Intracellular heterogeneity in mitochondrial membrane potentials revealed by a J-aggregate-forming lipophilic cation JC-1. *Proc. Natl. Acad. Sci. USA* **1991**, *88*, 3671–3675. [[CrossRef](#)]
38. Sabharwal, S.S.; Schumacker, P.T. Mitochondrial ROS in cancer: Initiators, amplifiers or an Achilles' heel? *Nat. Rev. Cancer* **2014**, *14*, 709–721. [[CrossRef](#)] [[PubMed](#)]
39. LeBel, C.P.; Ischiropoulos, H.; Bondy, S.C. Evaluation of the probe 2',7'-dichlorofluorescein as an indicator of reactive oxygen species formation and oxidative stress. *Chem. Res. Toxicol.* **1992**, *5*, 227–231. [[CrossRef](#)]
40. Mussunoor, S.; Murray, G.I. The role of annexins in tumour development and progression. *J. Pathol.* **2008**, *216*, 131–140. [[CrossRef](#)]
41. Li, J.; Yuan, J. Caspases in apoptosis and beyond. *Oncogene* **2008**, *27*, 6194–6206. [[CrossRef](#)] [[PubMed](#)]
42. Swanton, E.; Savory, P.; Cosulich, S.; Clarke, P.; Woodman, P. Bcl-2 regulates a caspase-3/caspase-2 apoptotic cascade in cytosolic extracts. *Oncogene* **1999**, *18*, 1781–1787. [[CrossRef](#)] [[PubMed](#)]

Disclaimer/Publisher's Note: The statements, opinions and data contained in all publications are solely those of the individual author(s) and contributor(s) and not of MDPI and/or the editor(s). MDPI and/or the editor(s) disclaim responsibility for any injury to people or property resulting from any ideas, methods, instructions or products referred to in the content.